NASA TECHNICAL MEMORANDUM

NASA TM X-58079
November 1971

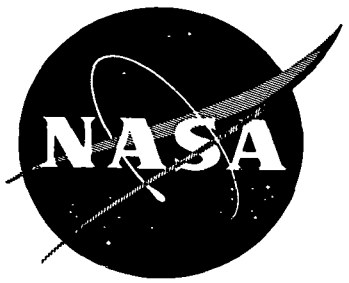

METEOROID ACTIVITY ON THE LUNAR SURFACE FROM THE SURVEYOR III SAMPLE EXAMINATION

Invited paper to XIVth Plenary Meeting COSPAR
Seattle, Washington
June 1971

NATIONAL AERONAUTICS AND SPACE ADMINISTRATION

MANNED SPACECRAFT CENTER

HOUSTON, TEXAS 77058

NASA TM X-58079

METEOROID ACTIVITY ON THE LUNAR SURFACE FROM THE SURVEYOR III SAMPLE EXAMINATION

B. G. Cour-Palais, H. A. Zook,
and R. E. Flaherty
Manned Spacecraft Center
Houston, Texas

METEOROID ACTIVITY ON THE LUNAR SURFACE FROM THE SURVEYOR III SAMPLE EXAMINATION

B. G. Cour-Palais, H. A. Zook, and R. E. Flaherty
NASA Manned Spacecraft Center
Houston, Texas U.S.A.

Abstract: The Surveyor III television camera shroud and polished aluminum tube, retrieved as a result of the Apollo 12 mission after 2-1/2 years on the lunar surface, were examined at the NASA Manned Spacecraft Center for evidence of meteoroid impact. The results of this examination indicate that the upper limit of meteoroid activity on the moon ranges between 3.3×10^{-6} m^{-2} s^{-1} for particles $\geq 10^{-9.2}$ gram and 1.7×10^{-6} m^{-2} s^{-1} for particles $\geq 10^{-7.85}$ gram. These values are compared with other estimates of the meteoroid flux in the lunar vicinity and are shown to be in good agreement with the Lunar Orbiter penetration rates. In addition, the relationship between a derived lunar-surface meteoroid cumulative-flux model and the comparable near-earth model is discussed in the light of theoretical predictions. It is shown that the effect of the gravitational field of the earth on the near-earth environment was greater than previously predicted. The implication is that the average meteoroid velocity relative to the earth is probably 17 km s^{-1}. The many low-velocity impacts on the Surveyor III camera and tube are shown to be of lunar-surface origin and to be primarily the result of rocket-exhaust interaction.

1. Introduction

The Apollo 12 mission plan included the return of a number of samples obtained from the Surveyor III spacecraft, which had landed on the moon

2-1/2 years earlier. Among the samples retrieved were the television camera and a 19.7-centimeter length of a polished aluminum tube, which was cut from one of the radar-antenna support struts. The tube was nonuniformly coated with a brownish deposit. The authors examined these components for evidence of meteoroid and lunar-ejecta damage after the normal sample quarantine period had elapsed. This examination took place in the NASA Manned Spacecraft Center (MSC) Lunar Receiving Laboratory between January 10 and 15, 1970.

At the end of the examination period, the polished aluminum tube was cut into six sections [1]. Sections B and C were retained at MSC for detailed analyses by the authors, and the remainder of the Surveyor samples were returned to the Hughes Aircraft Company facility in California. The sections, each approximately 2.54 centimeters long, were adjacent and were cut from the less contaminated end of the tube. They were chosen because the earlier examination of the entire tube had indicated the presence of possible meteoroid craters.

This report describes the results of the examinations and the conclusions that were drawn by the authors with regard to the lunar-surface meteoroid environment.

2. Relevant Geometry

The Apollo 12 lunar module (LM) landed approximately 180 meters northwest of the Surveyor III spacecraft [2], and this closeness is dramatically shown in a photograph taken by the astronauts, fig. 1. It can be seen that the LM landed on the rim of the Surveyor III crater and is sitting on the horizon relative to the spacecraft. The front, flat surface of the television camera

is approximately parallel to a line joining the Surveyor III spacecraft and the LM, a fact which is confirmed by correlating some of the craters seen in the figure with craters in photographs taken earlier by the Surveyor III spacecraft [3]. This correlation puts the LM at a camera azimuth of approximately 90°. From the same source, it is apparent also that the camera is leaning toward the LM and that the horizon, in that direction, is at a camera elevation of 25°. A more detailed description of the relative positions of the various elements pertinent to this paper is available [4].

The radar-antenna support strut from which the polished tube was cut is indicated by the arrow in fig. 1. Although the position of the cuts and the orientation of the two ends are not known, the probable sequence of operations has been inferred by the Surveyor spacecraft contractor (Hughes Aircraft Company) as a result of detailed examinations of the severed ends and experiments duplicating the events on the lunar surface [1]. These inferences are:

1. That the cleaner end of the tube (section A) is uphill
2. That the apex at each end points away from the astronaut
3. That the brownish contamination is on the side facing toward the interior of the spacecraft

Some evidence [5] exists that the clean end of the tube may have been pointing in a direction opposite to that suggested by Hughes.

3. Examination Outline

The preliminary examination took place in a temporary laboratory set up in the Lunar Receiving Laboratory and was accomplished in 6 days. During this

time, approximately 0.11 square meter of the television camera-shroud surface area of nearly 0.2 square meter was scanned at 25× magnification, and every suspected impact crater was recorded. The remainder of the camera surface was scanned at lower magnifications to ensure that no significant meteoroid damage had been overlooked. In addition, the 19.7-centimeter-long and 1.27-centimeter-diameter polished aluminum tube was scanned carefully at a general level of 40× magnification. Local areas of interest were examined at much higher magnifications, and typical surface effects and suspected impact craters were photographed for documentary purposes.

After the strut was sectioned and the samples returned to Hughes Aircraft Company, the two 2.54-centimeter-long sections retained by MSC were examined in detail over a period of several months. First, the sections were scanned optically at 100× magnification; and, then, an extensive examination was performed with a scanning electron microscope (SEM). The objectives of the SEM analyses were as follows:

1. To determine the origin of craters found during the optical scan of the B and C tube sections

2. To perform a spot survey at high magnifications over the entire C section of the tube

3. To determine, by nondispersive X-ray analysis, the composition of material in the craters and on the surface of the tube

Samples of the polished strut and the painted surface of the camera shroud supplied by Hughes Aircraft Company also were examined optically to determine surface backgrounds for comparative purposes.

4. Results of Examination

4.1. Television camera shroud

Although the time available permitted only a quick look for obvious impact craters, it is certainly true to say that no significantly damaging impacts were found on the camera shroud.

Typical surface effects and suspected impact craters are shown in fig. 2. It is interesting to note that the paint surface differs around the periphery of the shroud. On the side facing toward the interior of the Surveyor spacecraft, the surface appears grainy as in the majority of the views in the figure. However, on the portions facing outward, the surface is cracked like a dry riverbed as may be seen in two of the frames. Several holes and craters appear at the junction of cracks or along the cracks, and these were not included in the tally of suspected impacts. In addition, evidence of a large number of shallow white craters covering the housing was found, with a definite concentration occurring around the periphery in a region directly in line with the LM. The cylindrical surface under the mirror head had 255 of these craters on the surface toward the LM and only two on the surface facing away from the LM. The craters were obviously fresh because the original white color of the painted surfaces, which had been discolored to a sandy brown, was displayed. Protuberances on the camera, such as screwheads and support struts, left dark shadows of unaffected paint on the camera pointing away from the LM.

Several of the craters that were identified as being of possible meteoroid impact origin because of their hypervelocity appearance are shown in fig. 2. In all, there were five such craters, ranging in size from 130 to 300 microns in diameter, although it is likely that not all of these were caused by

meteoroids because three of the suspected impacts occurred on the flat mirror gearbox housing, approximately 25 square centimeters of area.

The camera-shroud surface also showed evidence of low-velocity impacts of irregular shape, some with embedded particulate material. These appear as depressions in fig. 2 as opposed to the lipped, circular indentations that characterize the possible hypervelocity craters.

4.2. Polished aluminum tube

The polished aluminum tube obtained from the Surveyor III spacecraft was cut with a pair of long-handled shears with curved, overlapping blades. The cutting action partially flattened the ends of the tube as may be seen in fig. 3. This figure also shows an increase in contamination, which appears brownish to the unaided eye, toward the left-hand end of the tube. Under a microscope, the contamination also appears brown and seems to be composed, at least partially, of crystals ranging in size up to a few microns. A variation in the amount of the contamination one observes as the tube is rotated around the cylindrical axis also is evident. The 40× examination of the entire surface of the tube revealed only four craters larger than 25 microns in diameter that exhibited possible characteristics of hypervelocity impacts at low magnifications. These craters were on the two sections of the tube retained by MSC, and subsequent detailed examination at higher magnifications discounted a meteoroid origin. Although the detailed examination of sections B and C at magnifications up to 600× revealed no obvious meteoroid impacts, a large number of other craters and pits were found. Fig. 4 illustrates the number of craters 20 microns and larger in diameter that were observed in the field of view of an optical microscope at 100× magnification

(corresponding to an area of approximately 1 square millimeter). Counts were taken as a function of angle around the tube from a scribe line which had been ruled along the tube prior to cutting, and the histogram is an average of two trials on the B section of the tube. Because very high pit densities (up to 40 per field of view) obtained in two places were obviously associated with polishing scratches, they are not included. The reduced count rate around 170° from the scribe line is not considered significant.

A measure of the relative amounts of brown contamination on the B section as a function of angle around the tube also is shown in fig. 4. This curve was obtained by photographing the tube at each angular position as the tube was rotated and the lighting held constant. The contamination stood out in the photographs between the angles 100° and 280° and appeared to peak at approximately 190°. Outside of these angles, the B section was relatively clean. The relative ordinate heights of the contamination curve are significant only in that a high ordinate indicates photographic evidence of "high" contamination relative to an angular position with a low ordinate. A close association between the pitting rate and the density of the brown contamination is immediately evident.

The results of the SEM analyses can be summarized as follows.

1. No craters showed evidence of hypervelocity impact origin. (It had not been possible by optical methods alone to determine whether some of the smaller craters had hypervelocity impact characteristics.)

2. All of the craters examined appeared to be of low-velocity impact origin, and many of them contained residual material.

3. The spot survey of section C confirmed the pitting density results of the optical scans but added little new information.

4. Analysis of the material in the craters strongly indicated that most of it was of lunar origin.

5. The brown contamination on the surface did not give any "peaks" because no elements with X-ray energies below approximately 1 kilovolt are detected with the analyzer on the SEM used. Hence, the presence of elements like oxygen, nitrogen, carbon, and so forth would not have been detected in this analysis.

Fig. 5 is a composite optical and SEM photograph of three typical craters on the B section that were located 280° from the scribe line. The lack of a smooth, raised lip entirely around the central indentation obviously excludes a hypervelocity impact origin for these craters. On the contrary, the shapes of these craters clearly indicate that material at a relatively low velocity. perhaps a few hundred meters per second, impacted the tube. The largest crater is approximately 30 microns in diameter, and material is still embedded in it. An X-ray pulse-height analysis of this material showed it to be composed of silicon, calcium, and iron with significant traces of chromium and titanium. The lower left-hand view of fig. 6 illustrates a region of high pitting density at 220° from the scribe line on the B section. The crater in the center is approximately 8 microns in diameter, and the material in this crater has as its major components silicon, iron, calcium, and titanium. Titanium also was found in another crater on this tube. The white-appearing material in the other three craters in fig. 6 shows up dark brown under an optical microscope, and

the nondispersive X-ray analysis indicated an iron-calcium silicate composition. Because only six typical craters were analyzed extensively by the SEM nondispersive X-ray analysis, the significant amounts of titanium found in three of them is quite indicative of a lunar origin.

The crater shown in the upper left-hand view of fig. 6 at 170° from the scribe line initially presented some excitement. Its size is approximately 80 microns by 110 microns, one of the largest craters on the tube; and it contains "rods" 3.5 microns in diameter and 20 to 40 microns long. The SEM analysis subsequently revealed that the rods were identical in composition to the Beta cloth glass fibers in the astronauts' outer garments and in the backpack in which the retrieved Surveyor III parts were stowed. Experiments at MSC have shown that it is possible to break off a few fibers by jamming the end of a strand of Beta fiber into a crater of this size.

The mineralogical analysis of the material in the craters shows complete consistency with lunar soil [5].

5. Discussion

5.1. Low-velocity impacts

When the Surveyor III camera is viewed from the direction of the LM, shadowed areas not whitened by cratering are alined directly behind protuberances such as bolts, screwheads, and other parts of the camera. These shadows are noticeable on the mirror hood, on the base of the camera where it was partly shielded by a plate, and near the screwheads on the mirror gearbox as shown enlarged in fig. 7. Note that the shadows are very well defined and that numerous white surface craters are found outside of the shadowed region,

indicating a "point" source. It is a simple matter to show by geometry that the origin of the particles responsible for the sandblasting of the television camera shroud is in the direction of the LM. Thus, it is postulated that, during the 2-1/2 years that the Surveyor III spacecraft rested on the moon, the white surface of the camera became discolored and that dust accelerated by the LM as it landed sandblasted the Surveyor spacecraft, removing much of the discoloration except in areas that were shielded. The sharpness of the shadows created by the shielding and their direction indicate that the path of the lunar dust was only slightly curved by lunar gravity, suggesting that it was traveling in excess of 100 m s^{-1}.

The close association between the brown contamination and the pits on section B of the polished tube and the fact that the pits contain lunar material indicate that this phenomenon occurred while the Surveyor III spacecraft was on the moon. Three of the possibilities considered as the origin follow.

1. Lunar secondary and tertiary ejecta stirred up by primary meteoroid impacts bombarded the exposed area of the tube to cause the pitting. The contamination also is composed of lunar material.

2. The pitting was caused by lunar material blasted toward the Surveyor III spacecraft by the LM as it landed.

3. The pitting was caused by lunar material blasted toward the tube by the Surveyor III spacecraft vernier thrusters, and the contamination was caused by incompletely burned propellant (unsymmetrical dimethylhydrazine monohydrate combined with nitrogen tetroxide oxidizer with a little nitrous oxide added as a catalyst).

Of these three possibilities, it would seem most likely that the material on the polished tube was transported form the lunar surface by either the LM descent-stage engine or the Surveyor III spacecraft vernier thrusters. Because the propellants used are nearly identical, the brownish contamination could have come from either source. The Surveyor III spacecraft vernier thrusters are thought to be the most probable cause of the low-velocity impacts and the contamination on the tube. A more detailed discussion leading to this conclusion is provided in ref. [5].

5.2. Meteoroid impacts

Because no meteoroid impacts were found on the tube for an exposure of 942 days, it is possible to set upper limits to the meteoroid flux at the moon. The detection threshold over the entire tube corresponds to craters approximately 50 microns in diameter. The highly contaminated region was sufficiently pitted and scarred as to make it impracticable to resolve features of smaller craters. On the nonpitted sides of sections B and C, the detection threshold corresponds to 25-micron-diameter and larger craters. The effective area of the nonpitted region is approximately half the area of these sections. If it is assumed that meteoroid impact craters are hemispherical in shape in the 2024-T3 aluminum alloy tube, then the threshold penetration depths are, respectively, 25 microns over the entire tube and 12.5 microns over one-half

of each of the two 1-inch sections. Using a hypervelocity penetration equation for 2024 aluminum developed by Cour-Palais at MSC,

$$P = 0.34 d^{1.06} \rho^{0.5} V^{0.67}$$

where P = crater depth, centimeters

d = meteoroid diameter, centimeters

ρ = meteoroid mass density, g cm^{-3}

V = meteoroid velocity, km s^{-1}

the 50-micron-diameter threshold corresponds to a meteoroid 14.6 microns in diameter and a mass of $10^{-8.79}$ gram. Similarly, the 25-micron-diameter threshold corresponds to a meteoroid 7.6 microns in diameter and a mass of $10^{-9.64}$ gram. These masses were derived for a 20-km s^{-1} impact velocity and a 1-g cm^{-3} mass density.

The area of the entire tube is approximately 78.5 square centimeters, and the area of the nonpitted regions of the B and C sections is 10.1 square centimeters. Using a shielding factor of 0.5 resulting from the moon and another factor of 0.67 resulting from the fact that the Surveyor spacecraft cuts out approximately one-third of the remaining solid angle from which meteoroids could approach, the effective area-times are 2.16×10^5 m^2 s for the entire tube and 0.28×10^5 m^2 s for the nonpitted regions of the B and C sections. The 95-percent upper confidence limits on the meteoroid flux for no impacts [6] for these exposures are $10^{-4.75}$ m^{-2} s^{-1} and $10^{-3.88}$ m^{-2} s^{-1}, respectively.

The diameters of the five craters found on the camera-shroud surface are given in table 1. The cumulative total number for each size and larger and the

corresponding 95-percent upper and lower confidence limits [6] also are included. Table 2 shows the associated cumulative fluxes based on a moon-shielding factor of 0.5 and a spacecraft-shielding factor of 0.75, assuming that the Surveyor III spacecraft shields one-fourth of the remaining solid angle. The meteoroid masses given for each size were based on the assumption that the crater-diameter-to-meteoroid-diameter ratio is 10 for the camera-shroud surface. The ratio chosen was obtained by the authors from laboratory hypervelocity impact data for targets of widely varying ductility.

The meteoroid flux at the lunar surface obtained from the polished tube and from the television camera shroud is plotted in fig. 8 in relation to the flux estimates obtained from the Surveyor III spacecraft footpad imprint [7] and from the Lunar Orbiter meteoroid experiments [8]. The Lunar Orbiter meteoroid experiments measured penetration rates in lunar orbit by using 0.0025-centimeter beryllium-copper pressurized-cell detectors, the same type of detector used on the Explorer 16 and 23 spacecraft for penetration-rate measurements in near-earth orbit [8]. The minimum meteoroid mass capable of perforating the 0.0025-centimeter beryllium-copper pressure cell, assuming a 20-km s^{-1} impact and a 0.5-g cm^{-3} mass density, is 10^{-9} gram [9]. The minimum discernible crater in the Surveyor III spacecraft footpad imprint was calculated to be one that would have been caused by a 3×10^{-8} gram meteoroid at an impact velocity of 20 km s^{-1} [7]. Because no craters of this limiting size or larger were found, the 95-percent upper confidence limit of 3.7 [6] has been used. The associated flux seen in fig. 8 includes a factor of 0.8 to account for shielding of the available solid angle by the Surveyor spacecraft and the footpad imprint walls. Fig. 8 also shows a portion of a corresponding

near-earth flux estimate with the pertinent experiment data points. This estimate is taken from the near-earth meteoroid environment model of ref. [9].

It is evident that the Surveyor III camera-shroud results are in good agreement with the Lunar Orbiter data and that the flux in the vicinity of the moon is lower than that near earth. It is apparent also that the statistical upper-limit flux values for the zero-meteoroid impacts detected on the Surveyor III spacecraft polished tube and footpad imprint are too high to demonstrate a decrease compared with the near-earth flux estimate chosen. As the statistically more significant Lunar Orbiter and Surveyor III camera-shroud data cover approximately the same meteoroid mass range, the polished-tube data will be ignored for the remainder of this paper. However, the Surveyor III spacecraft footpad imprint result, based on an upper limit of one impact as in ref. [7], will be used.

The four Surveyor III camera-shroud data points and the Lunar Orbiter data point are shown on an expanded scale in fig. 9. The mass of the latter has been recomputed by assuming a meteoroid density of 1 g cm^{-3}, which is the value used for the Surveyor III crater-mass determinations. This computation results in a slightly smaller meteoroid mass of $10^{-9.18}$ gram instead of the previously calculated 10^{-9} gram [9], and the effect is to make the Lunar Orbiter flux even more consistent with the Surveyor III camera-shroud results. The Surveyor III spacecraft footpad imprint flux upper limit is seen to be quite compatible with the camera-shroud data. The solid curve in fig. 9 represents the derived lunar-surface meteoroid flux based on the near-earth meteoroid environment model of ref. [9] as decreased by a gravitational factor

of 0.56, which is also discussed in the same reference. Fig. 9 also shows the least-squares fit to the Lunar Orbiter data and the Surveyor III camera-shroud data.

It is apparent that the factor of 0.56 applied to the near-earth flux does not decrease it enough to give agreement with the measured flux on and near the lunar surface. The slopes of the two flux-mass curves do, however, agree in the mass range shown; and, therefore, the two fluxes should agree if the appropriate gravitational reduction is applied to the near-earth data. The gravitational decrease factor is a function of the assumed meteoroid-velocity distribution; and, therefore, a determination of this factor gives important information about the meteoroid-velocity distribution function.

The gravitational factor for a flux determined near earth has been shown by D. J. Kessler at MSC to depend on the assumed meteoroid-velocity distribution at the edge of the earth's atmosphere as

$$G = 1 - V_e^{2} \cdot V_n^{-2} \cdot (1 - r_e \cdot r^{-1})$$

where V_e = earth escape velocity, km s^{-1}

r_e = earth radius, kilometers

r = distance from center of earth, kilometers

V_n = a representative velocity equal to $(\bar{V}^n)^{1/n}$, km s^{-1}

where $\bar{V}^n = \int V^n f(v)\, dv$

$f(v)$ = the normalized meteoroid-velocity distribution function at the edge of the earth's atmosphere

$n = -2$

The calculated value of G is 0.56 at the lunar distance based on a gravitationally influenced geocentric meteoroid-velocity distribution for which the near-earth average is 20 km s^{-1} [9], and the corresponding near-lunar and representative velocity V_n are 19.5 and 16.8 km s^{-1}, respectively.

Because the Lunar Orbiter spacecraft had the same type of detectors as were used for the Explorer 16 and 23 spacecraft in near-earth orbit, the ratio of puncture rates is closely indicative of the gravitational factor. Because the meteoroid environment flux model of ref. [9] does not pass precisely through the Explorer 16 and 23 points, it is not as suitable for comparing with lunar data to obtain a gravitational decrease factor. Thus, the five Lunar Orbiter spacecraft recorded a penetration flux of 2.2×10^{-6} m^{-2} s^{-1}, and the Explorer spacecraft recorded an average rate of 5.33×10^{-6} m^{-2} s^{-1} in earth orbit [8]. The corresponding experimentally determined gravitational factor to be applied to the near-earth flux is 0.41. The difference between the derived value of 0.56 and the measured value of 0.41 cannot be accounted for by the fact that the former is based on a mass flux and the latter on a penetration flux. The reason is that the average velocities near earth and at lunar distances are almost identical for the velocity distribution given in ref. [9]; that is, 20 and 19.5 km s^{-1}, respectively. However, according to Kessler [10], a meteoroid-velocity distribution for which the average gravitationally influenced geocentric or near-earth velocity is 17 km s^{-1} and the average at lunar distances is 15.2 km s^{-1}, reproduced as fig. 10, results in a mass flux at the moon that is 0.48 of that near earth. If the Explorer and Lunar Orbiter penetrating masses are recalculated for these two average velocities, the resulting measured gravitational decrease factor based on mass flux is 0.47.

Thus, the calculated and measured values are in agreement if Kessler's velocity distributions are used.

6. Conclusions

Although the Surveyor III camera-shroud meteoroid data cannot be considered as having resulted from a controlled experiment, they are meaningful when considered in conjunction with the Lunar Orbiter results. The conclusions reached after analyzing the results of the Surveyor III camera-shroud and polished-tube examination, together with the statistically more significant Lunar Orbiter data, may be summarized as follows.

1. The meteoroid flux at the lunar surface resulting from an analysis of five probable impacts observed on the camera shroud is in good agreement with the penetration rate measured by five Lunar Orbiter spacecraft.

2. The slope of the lunar-surface meteoroid cumulative-mass distribution, for the mass range measured by the combined Lunar Orbiter-Surveyor shroud results, is in good agreement with the near-earth model described in ref. [9].

3. The unshielded meteoroid flux on the lunar surface, determined from the combined Lunar Orbiter-Surveyor shroud results, is:

$$\log_{10} N\left(m^{-2}\ s^{-1}\right) = -10.80 - 0.56 \log_{10} m(g)$$

for the meteoroid mass (m) range 5×10^{-10} gram $\leq m \leq 2 \times 10^{-8}$ gram. The 95-percent upper limit for this meteoroid activity ranges between 3.3×10^{-6} m^{-2} s^{-1} for particles $\geq 10^{-9.18}$ gram and 1.7×10^{-6} m^{-2} s^{-1} for particles $\geq 10^{-7.85}$ gram.

4. The lunar-surface meteoroid flux derived from the near-earth flux model and gravitational factor (0.56) of ref. [9] is higher than the measured

flux determined by the Lunar Orbiter-Surveyor shroud results. The probable explanation for the lower than predicted lunar-surface flux is that the meteoroid-velocity distribution function used in the calculations is somewhat in error. A velocity distribution that allows the lunar-surface meteoroid flux derived from ref. [9] to agree with the measured Lunar Orbiter-Surveyor flux is given by Kessler in ref. [10]. The average near-earth and lunar-surface velocities of this distribution are 17 and 15.2 km s^{-1}, respectively. The associated meteoroid flux at the lunar surface thus would be 48 percent of that near-earth instead of 56 percent.

References

[1] ANON., Hughes Aircraft Company Technical Report No. P70-54 (1971).

[2] ANON., NASA Special Publication SP-235 (1970).

[3] ANON., NASA Special Publication SP-146 (1967).

[4] N. L. NICKLE, in: Proc. Apollo 12 Lunar Science Conf., Geochim. Cosmochim. Acta Supp., Massachusetts Institute of Technology Press, Cambridge, Massachusetts 1971.

[5] B. G. COUR-PALAIS et al., in: Proc. Apollo 12 Lunar Science Conf., Geochim. Cosmochim. Acta Supp., Massachusetts Institute of Technology Press, Cambridge, Massachusetts 1971.

[6] W. E. RICKER, J. Am. Stat. Assoc. 32, 349 (1937).

[7] L. D. JAFFE, Science 170, 1092 (1970).

[8] G. W. GREW and C. A. GURTLER, NASA Technical Note D-6266 (1971).

[9] ANON., NASA Special Publication SP-8013 (1969).

[10] D. J. KESSLER, AIAA J. 7, 2337 (1969).

Table 1

Number of probable meteoroid craters in camera shroud

Crater diameter, D_c (cm)	Number, N	ΣN, $\geq D_c$	95% upper and lower limits
1.3×10^{-2}	1	5	11.7 1.6
1.5×10^{-2}	1	4	10.2 1.0
2.33×10^{-2}	2	3	8.8 0.6
3.00×10^{-2}	1	1	5.6 0.1

Table 2

Calculated flux, diameter, and mass for craters in camera shroud

Crater diameter, D_c (cm)	Cumulative flux (m^{-2} s^{-1})	Meteoroid diameter, d (cm)	Meteoroid mass, m (g)
1.3×10^{-2}	1.49×10^{-6}	1.3×10^{-3}	1.15×10^{-9}
1.5×10^{-2}	1.19×10^{-6}	1.5×10^{-3}	1.77×10^{-9}
2.33×10^{-2}	8.94×10^{-7}	2.33×10^{-3}	6.63×10^{-9}
3.00×10^{-2}	3.0×10^{-7}	3.00×10^{-3}	1.41×10^{-8}

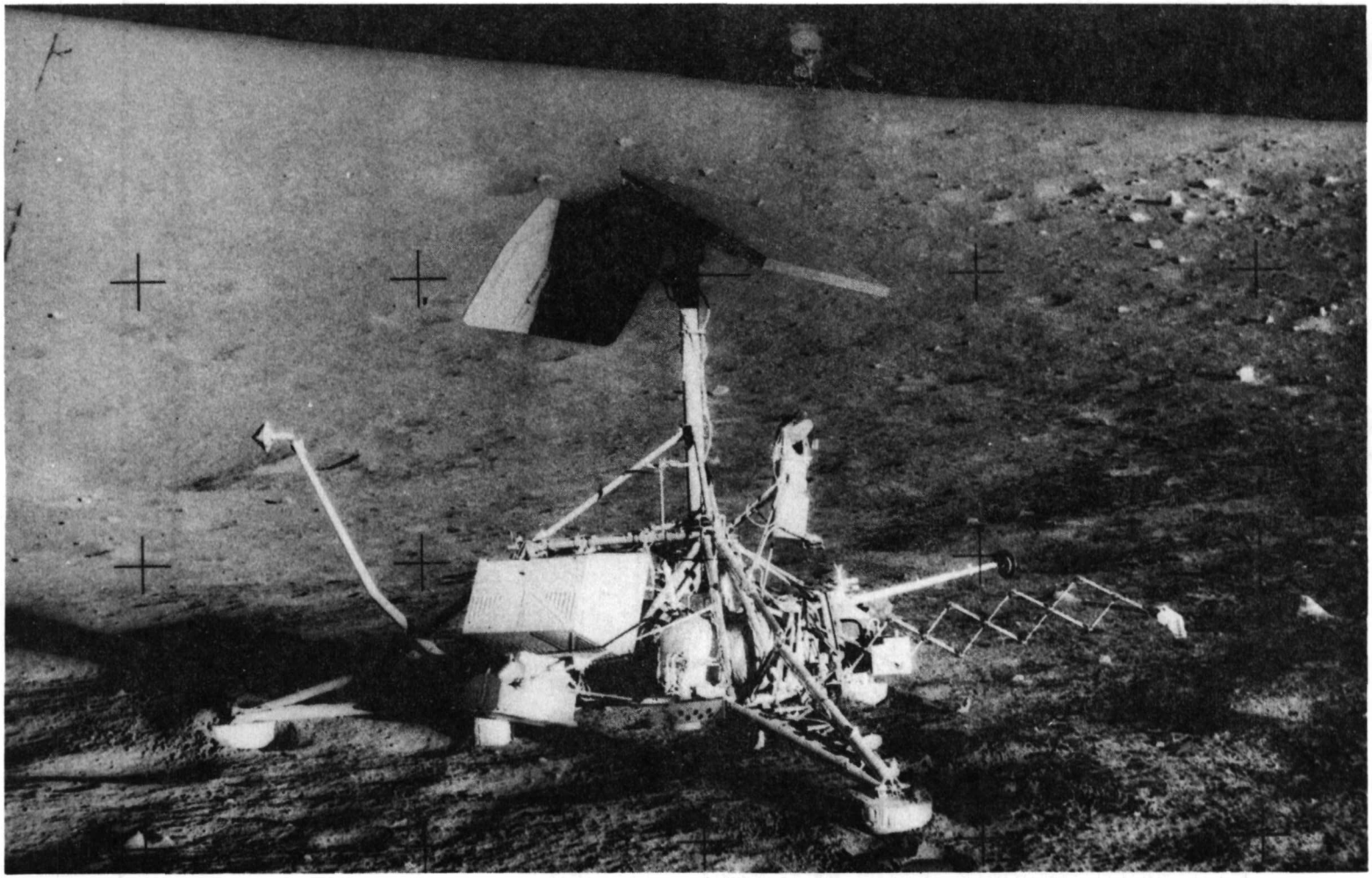

Fig. 1. A view of the Apollo 12 LM from the Surveyor III landing site. The arrow points to the radar-antenna support strut from which the polished-tube section was cut.

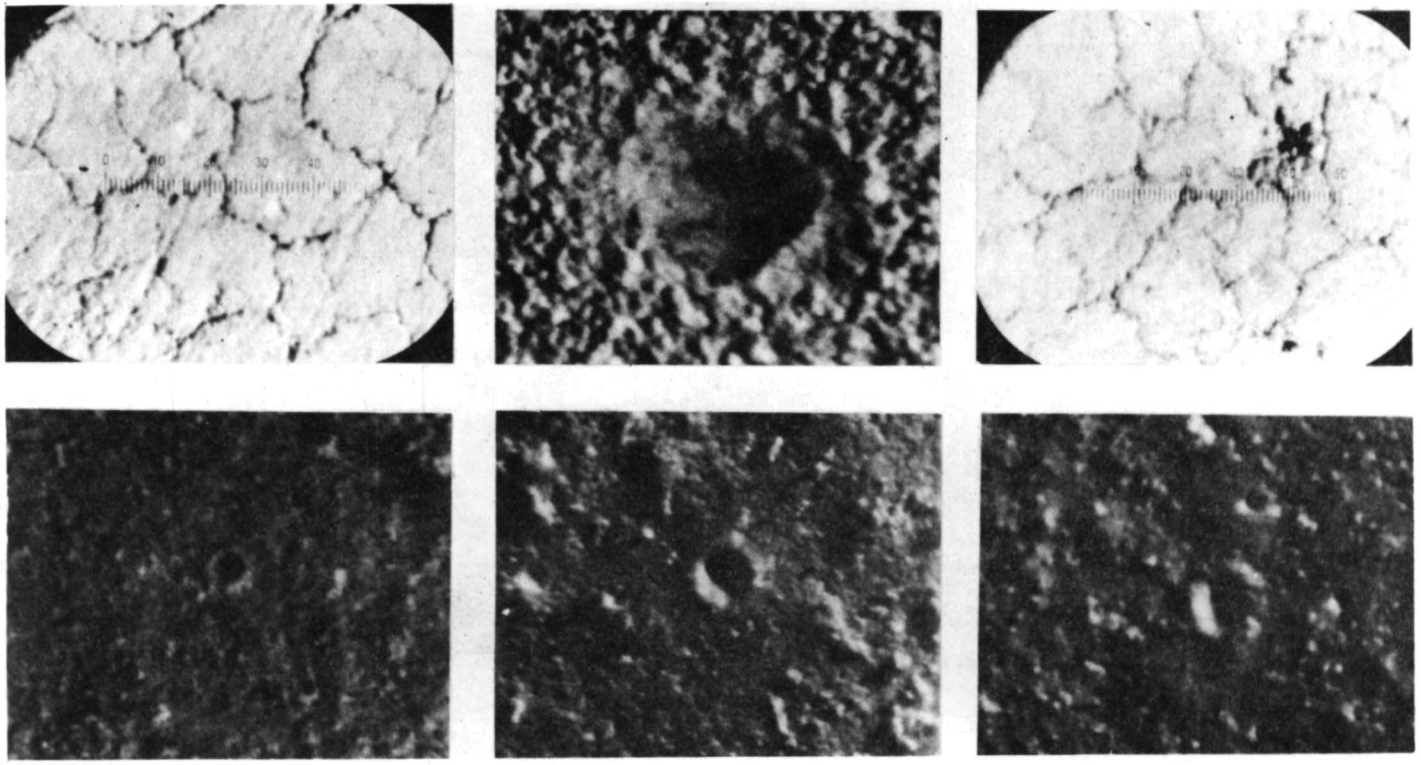

Fig. 2. Surface features found on the Surveyor III camera shroud.

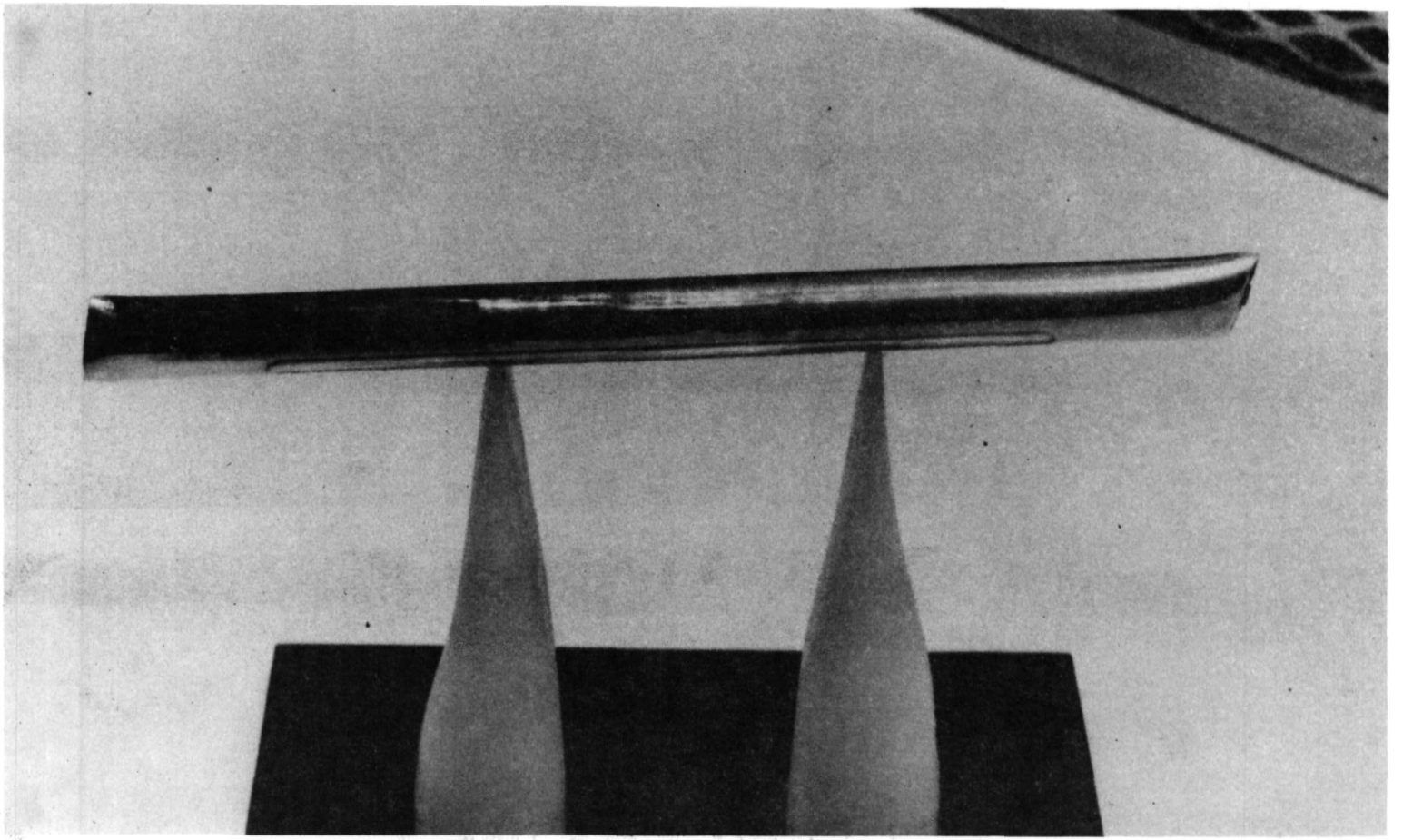

Fig. 3. The polished aluminum tube section obtained from the Surveyor III spacecraft, showing the contamination darkening to the left. Sections B and C were cut 3.8 centimeters in from the right-hand end.

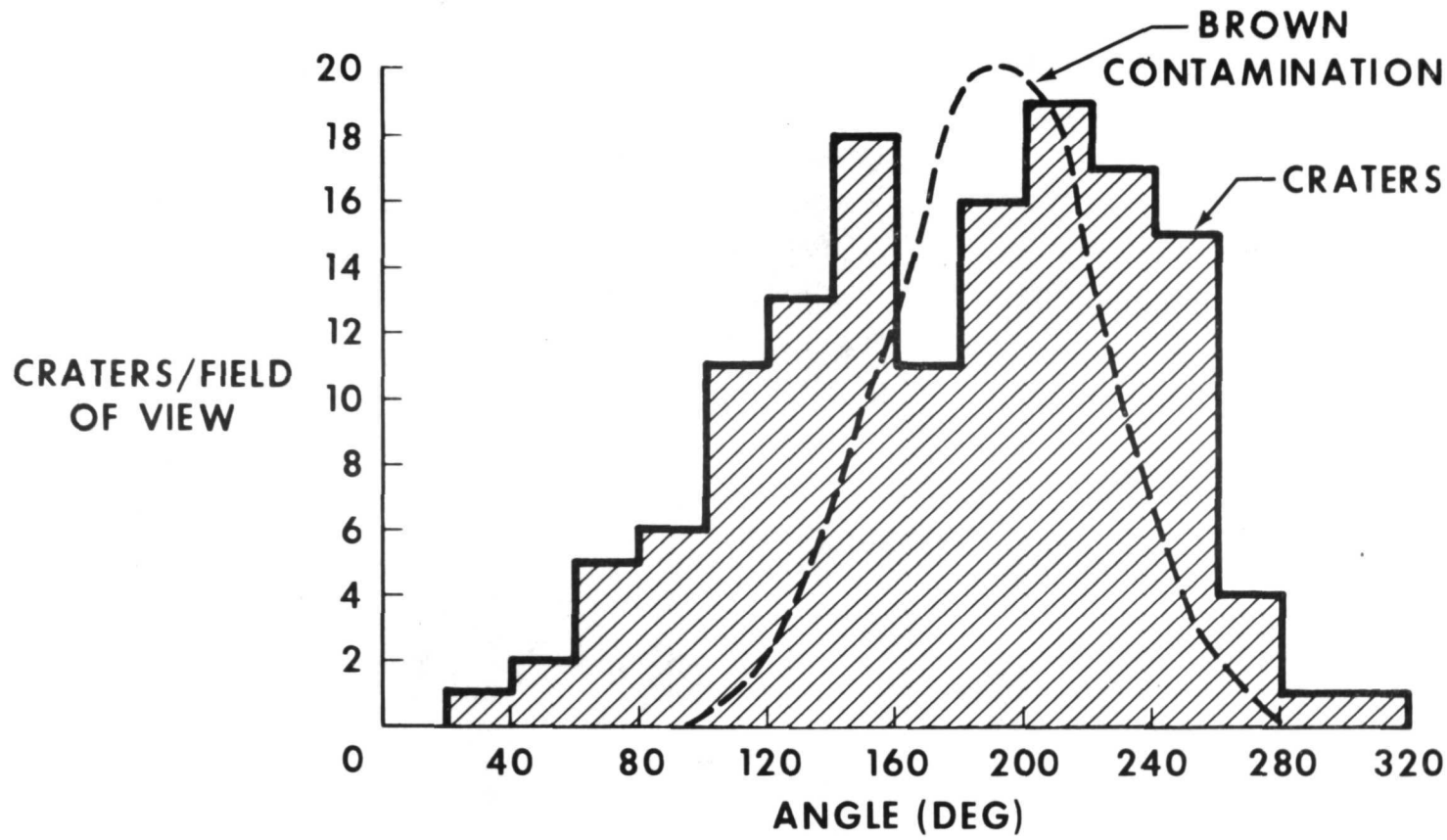

Fig. 4. Distribution of the contamination and low-velocity surface effects on sections B and C of the polished tube.

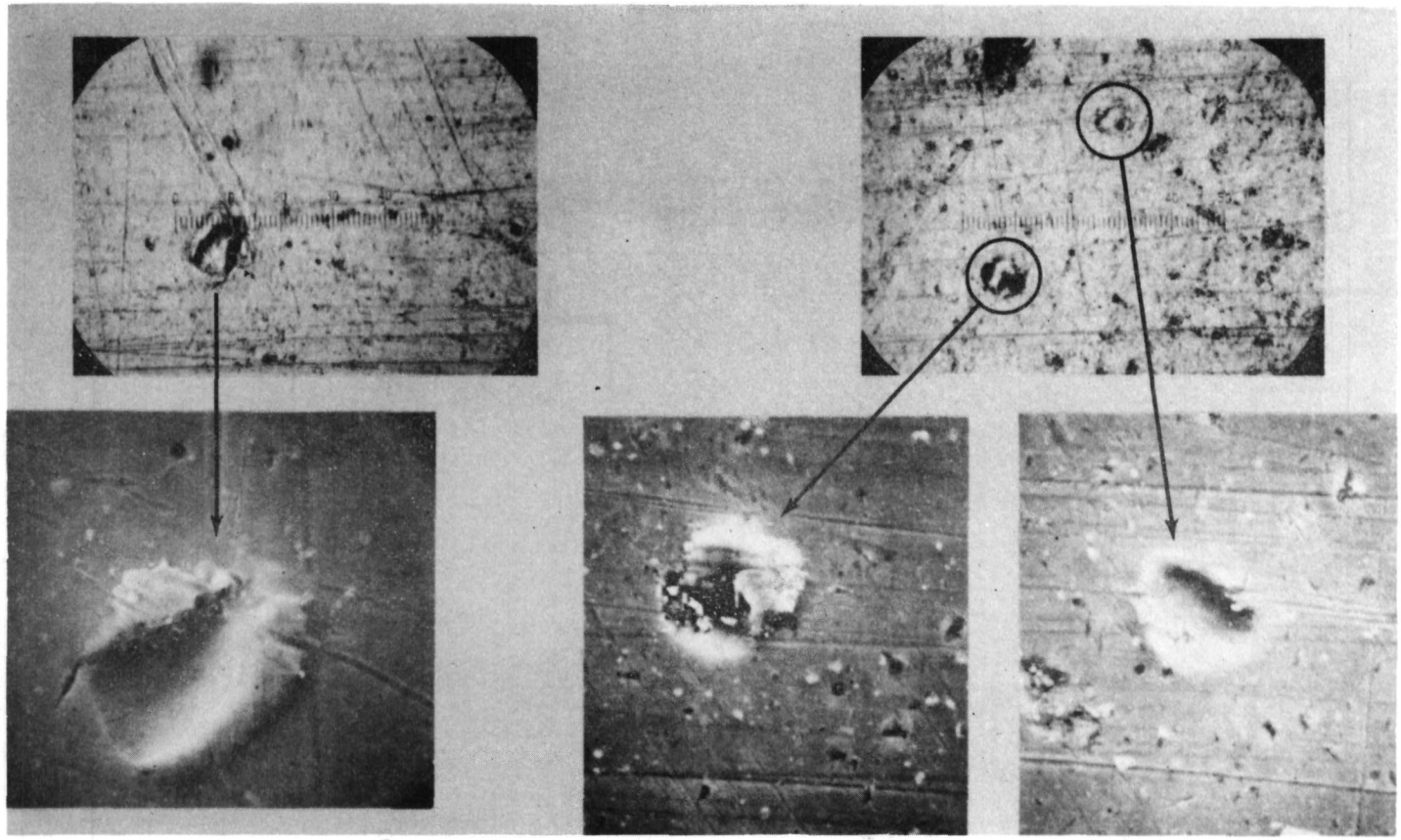

Fig. 5. Optical and SEM views of typical impact effects on sections B and C of the polished tube. The arrows point to related craters in the lower views.

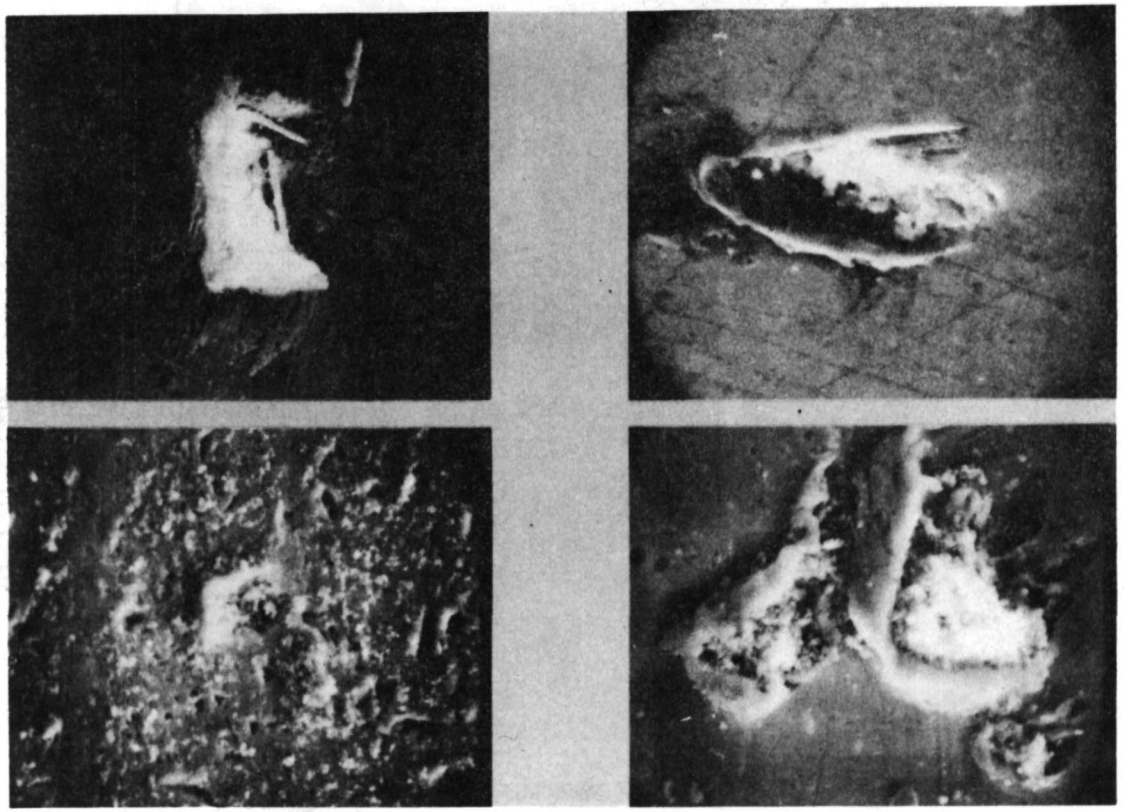

Fig. 6. Evidence of debris within some of the impact effects found on sections B and C of the polished tube.

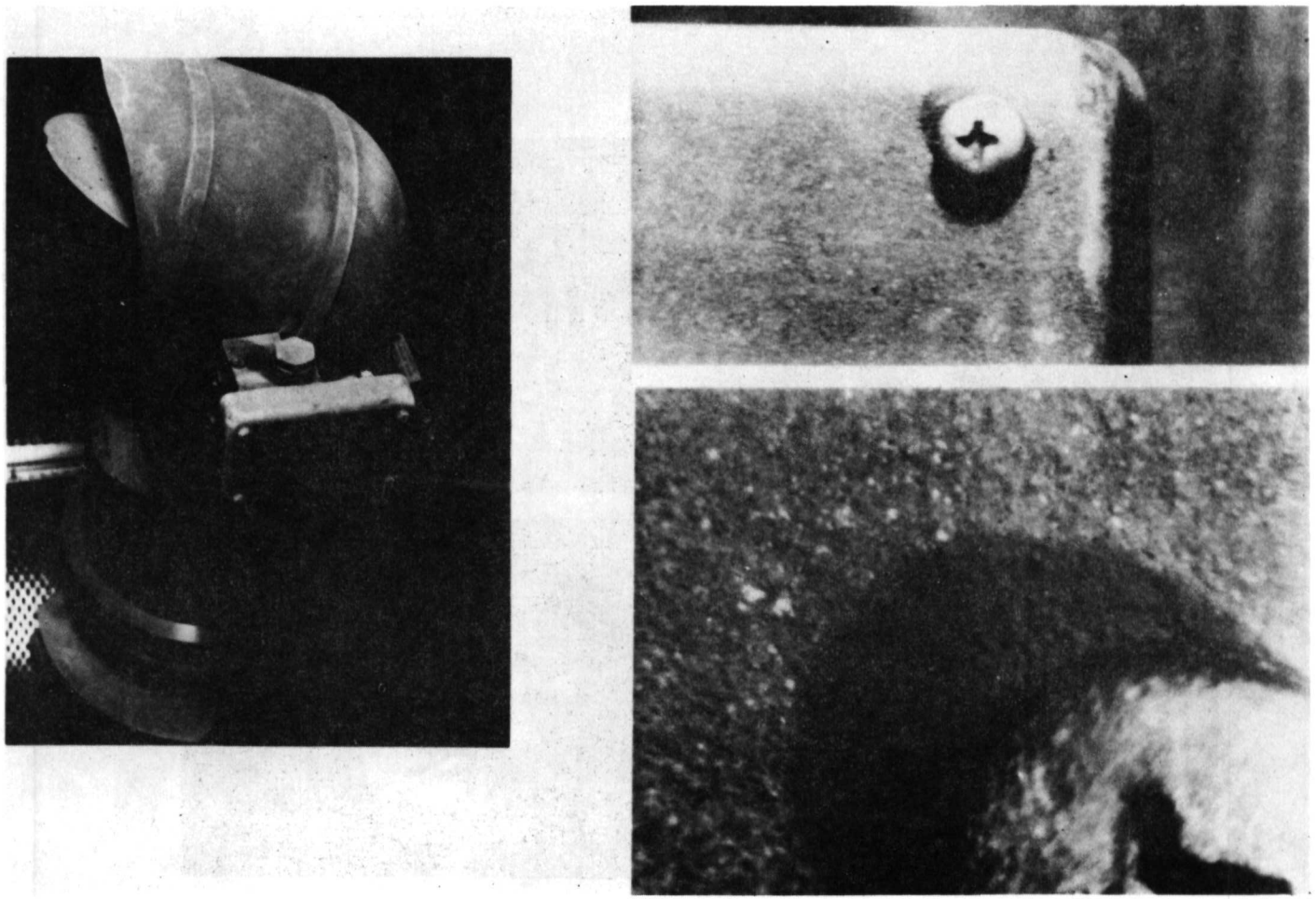

Fig. 7. Details of the shielding provided by the Surveyor III camera protuberances to the LM-exhaust lunar duststorm.

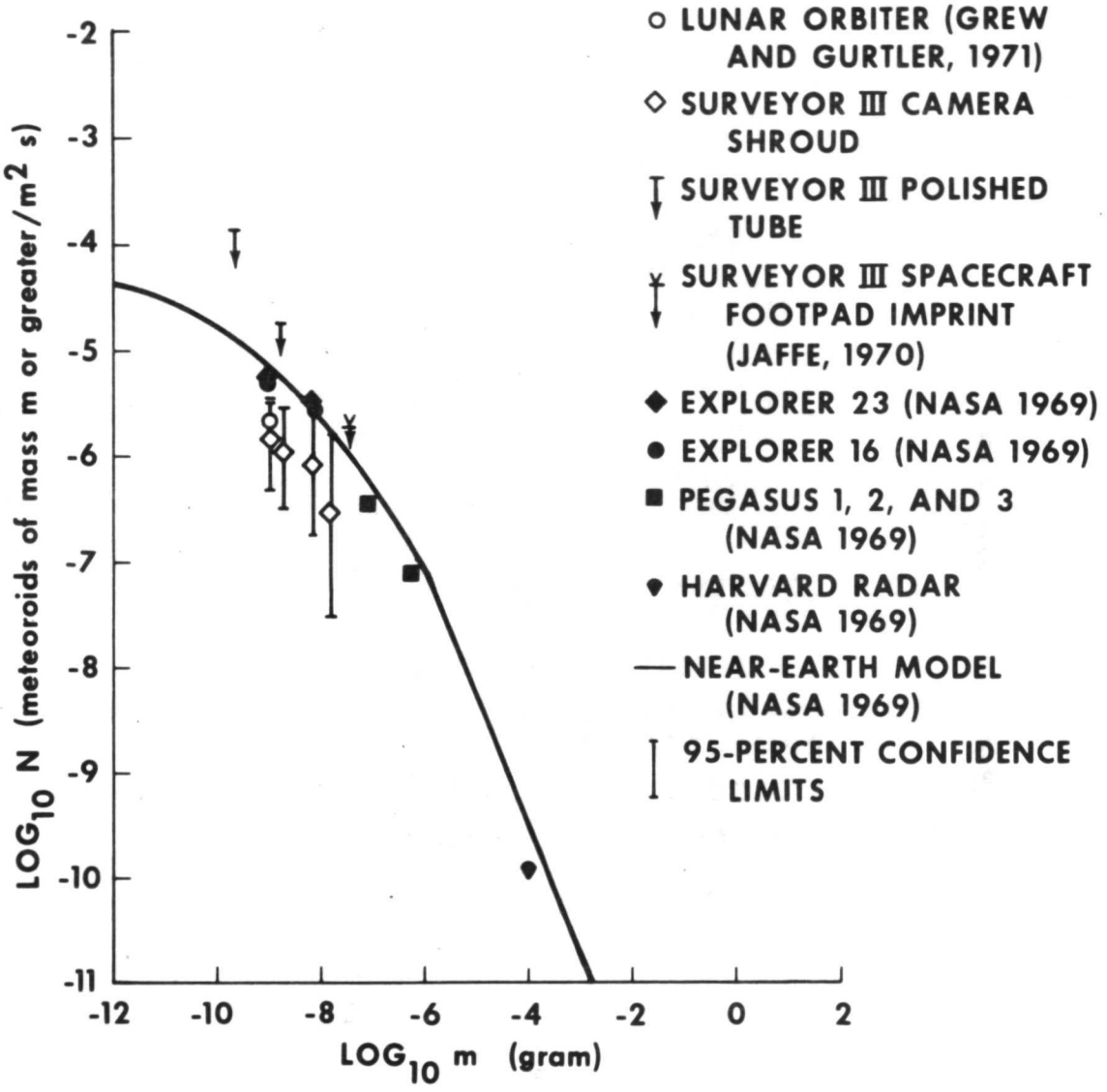

Fig. 8. Comparison of near-lunar flux with near-earth meteoroid model and data.

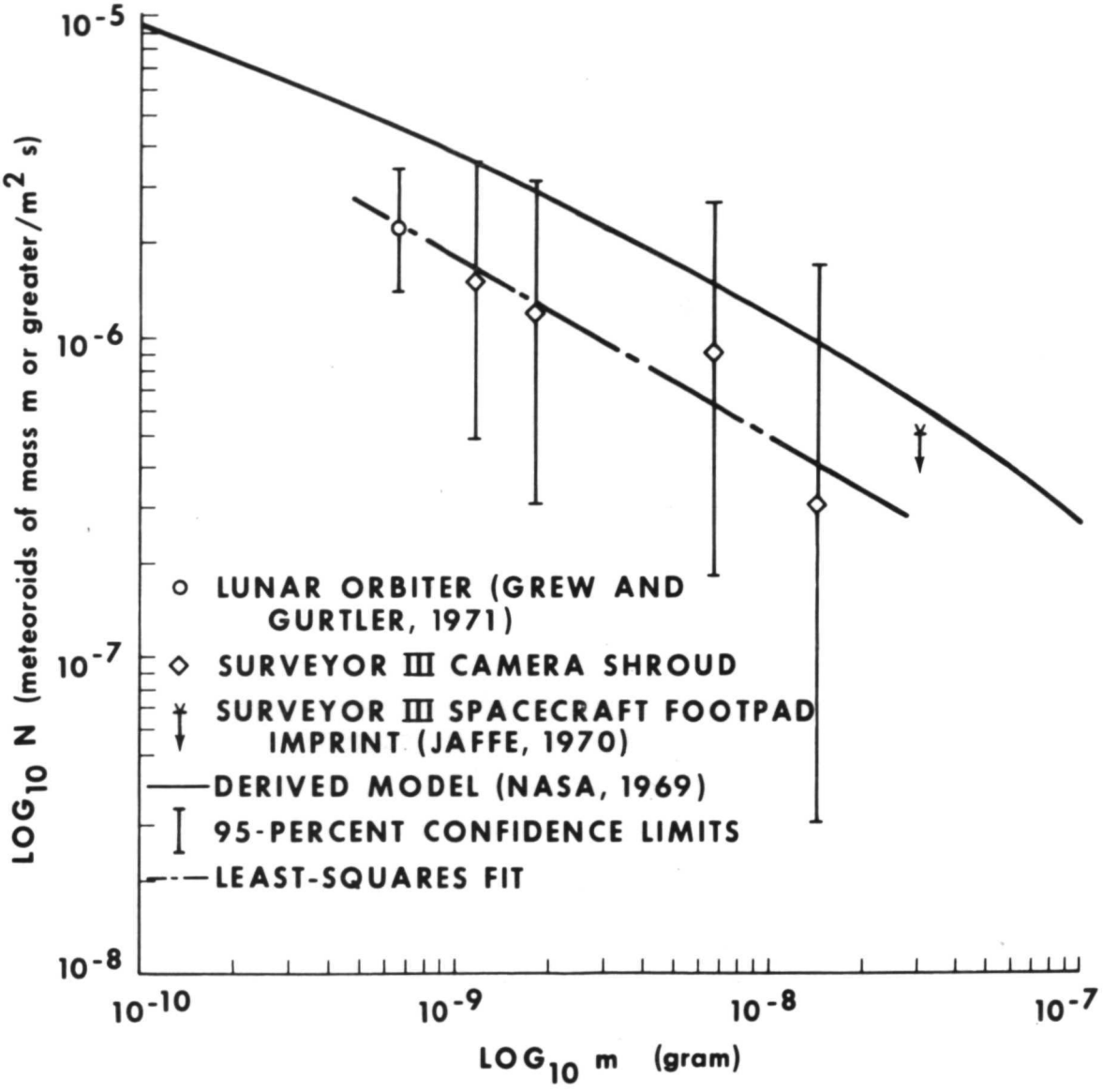

Fig. 9. Predicted and measured lunar-surface meteoroid activity.

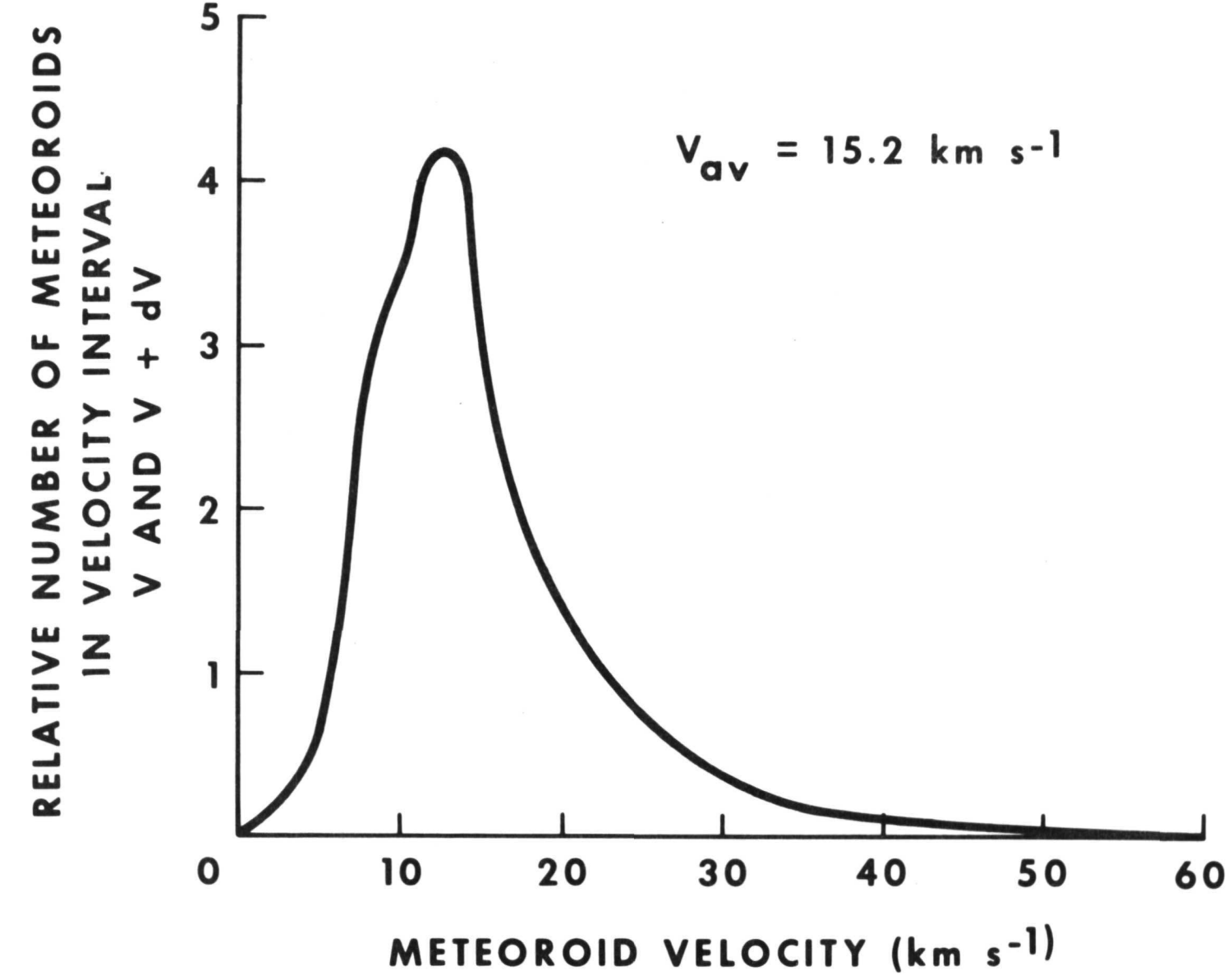

Fig. 10. Meteoroid-velocity distribution outside gravitational sphere of influence of the earth applied to the lunar surface.